IOP Publishing Superconductor Science and Technology
Supercond. Sci. Technol. **37** (2024) 075018 (10pp) https://doi.org/10.1088/1361-6668/ad5114

Enhancement of the critical current by surface irregularities in Fe-based superconductors

I F Llovo[1,2,3], J Mosqueira[1,2,*], Ding Hu[4], Huiqian Luo[5] and Shiliang Li[5]

[1] QMatterPhotonics Research Group, Departamento de Física de Partículas, Universidade de Santiago de Compostela, 15782 Santiago de Compostela, Spain
[2] Instituto de Materiais (iMATUS), Universidade de Santiago de Compostela, 15706 Santiago de Compostela, Spain
[3] Centro de Supercomputación de Galicia (CESGA), 15705 Santiago de Compostela, Spain
[4] School of Physics, Hangzhou Normal University, Hangzhou 311121, People's Republic of China
[5] Beijing National Laboratory for Condensed Matter Physics, Institute of Physics, Chinese Academy of Sciences, Beijing 100190, People's Republic of China

E-mail: j.mosqueira@usc.es

Received 21 October 2023, revised 28 April 2024
Accepted for publication 27 May 2024
Published 14 June 2024

Abstract

The critical current I_c of single crystals of the iron pnictide superconductor $BaFe_2(As_{1-x}P_x)_2$ has been studied through measurements of magnetic hysteresis cycles. We show that the introduction of micrometer-scale irregularities on the surface significantly increases I_c, primarily near the irreversibility magnetic field H_{irr}. The observed increase can be attributed to a non-dissipative surface current that arises from the collective bending of the vortex lattice at the sample surface, enabled by the surface irregularities. This mechanism, which is not pinning in the proper sense, has previously been studied in clean, low-T_c, metallic superconductors, but had not been investigated in Fe-based superconductors. The observed increase in I_c is consistent with a theoretical estimate based on the Mathieu-Simon continuum theory of the vortex state.

Supplementary material for this article is available online

Keywords: Fe-based superconductors, critical current, surface pinning, surface roughness, magnetic properties

1. Introduction

Since the 2008 discovery of superconductivity at high critical temperature in iron-based superconductors (FeSC) [1], intensive research on these materials has been taking place. On the one hand, these materials have a fundamental interest, as they share multiple similarities with high-T_c cuprates, such as elevated transition temperatures and the emergence of superconductivity with the introduction of dopants that destroy the antiferromagnetic order of the parent system [2–4], suggesting their pairing mechanism may be similar [5].

FeSC also present a multiband electronic structure [2–4], which leads to unconventional behavior of observables such as the magnetic penetration depth [6], the Seebeck coefficient [7], the specific heat [8, 9], or the upper critical field [10–13]. On the other hand, these materials present some properties that make them interesting from an applications perspective, such as high critical and irreversibility magnetic fields [14–18], and a relatively low anisotropy. The 122 family of iron-based superconductors is one of the most prominent candidates for next generation superconducting tapes and wires, as the compounds from this family show particularly low anisotropy and large grain boundary critical angle (as high as 9°), making them suitable for techniques such as powder-in-tube manufacture of wires and tapes [19–24], and for the development

* Author to whom any correspondence should be addressed.

of superconducting devices such as bulk magnets [25] or thin-film nanocircuits including integrated Josephson junctions and SQUIDs [20].

For the aforementioned reasons, much attention has been put on enhancing the critical current density J_c of these materials. Multiple techniques have been shown to serve this purpose, such as proton, neutron and heavy ion irradiation to produce point-like [26–28] or columnar [26, 27, 29–31] defects; optimizing the substrate conditions (in the case of thin films) [32, 33], the addition of self-assembled oxygen-rich impurities [34], and the artificial generation of compositionally modulated superlattices, e.g. $BaFe_2As_2/Ba(Fe_{1-x}Co_x)_2As_2$ [35]. In addition to bulk pinning, surface irregularities have also been shown to be effective at enhancing the critical current in conventional low-T_c superconductors [36, 37]. Among the procedures used to create surface defects in these materials are sandblasting [37], mechanical abrasion [38], buffered chemical or electrolytic polishing [39], and low temperature bakeout [40]. More recent work in metallic niobium sheets has shown that laser-induced periodic structuration can make the irreversibility field H_{irr} increase [41], or decrease when using a femtosecond-pulsed laser [42].

In this work, we investigate the effect of micrometric surface irregularities on the critical current I_c of FeSC single crystals. The 122 family is widely studied in applied research due to its lower anisotropy and higher critical current density J_c. [20] For this reason, we selected optimally-doped $BaFe_2(As_{1-x}P_x)_2$ (Ba122:P) for this study, as crystals of considerable dimensions and high stoichiometric quality can be grown [43–45]. A significant I_c increase is observed after the surface treatment, mainly near the irreversibility field H_{irr}, which is attributed to a non-dissipative surface current, in turn associated to a collective vortex bending near the sample surface. Such a bending is made possible by surface irregularities, which provide multiple ways for vortices to terminate on the surface while still satisfying boundary conditions. This mechanism has already been observed in clean low-T_c metallic superconductors [36, 37], but it is the first time it is studied in Fe-based superconductors. The results are compared with a theoretical estimate for the critical current density that a rough surface can sustain, based on the Mathieu-Simon continuum theory of the mixed state [36, 37].

2. Methods

2.1. Crystals growth and characterization

$BaFe_2(As_{1-x}P_x)_2$ ($x = 0.35$) single crystals were grown using the Ba_2As_3/Ba_2P_3 self-flux method described in [43]. They are platelike, with typical surfaces of several mm^2 and thicknesses up to ∼0.1 mm (see table 1). A thorough characterization of crystals from the same batch was presented in [45], where energy-dispersive x-ray analysis showed excellent compositional homogeneity, with a stoichiometric deviation of less than 0.4% between different crystals and different studied areas. The crystals used in this work are among those used in [45], and have been since kept in an epoxy matrix until the beginning of this study. Their crystallographic structure was analyzed by x-ray diffraction (XRD), using a Rigaku MiniFlex II diffractometer with a Cu target and a graphite Cu Kα monocromator. The reflections by the crystal *ab* planes (parallel to the FeAs layers) are presented in figure 1. The absence of reflections other than the (00ℓ) indicates the excellent structural quality of the crystals, and the resulting *c*-axis lattice parameter is about 12.80 Å (see table 1), in agreement with data in the literature for crystals with a similar As-P proportion [46–48].

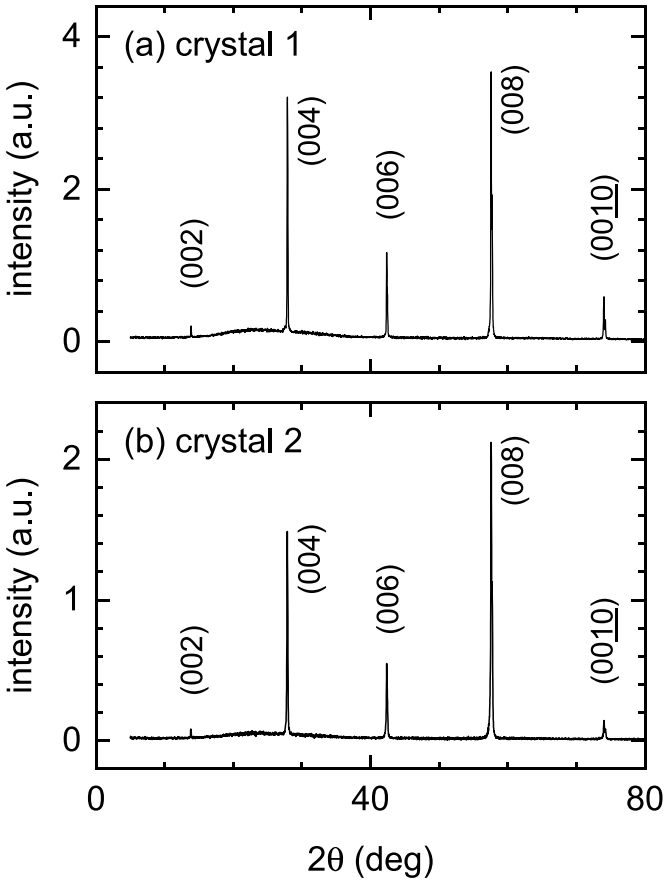

Figure 1. X-ray diffraction patterns of crystal 1 and crystal 2 before and after the treatment, respectively. The data were obtained using the geometry to observe the reflections by the *ab* layers. Only (00ℓ) diffraction peaks are present, evidencing the excellent structural quality of the crystals. Moreover, the positions and widths of the peaks are not visibly changed by the surface treatment, indicating that the structural quality of the crystals remains unaltered.

2.2. Surface etching process

The crystals were subjected to an abrasive sandblasting process to create micrometric irregularities on their surfaces. A commercial sandblasting machine (Damglass E. Fexas, DAM-1) was used with silica sand of diameter ∼50–100 μm. The samples were kept centered in the ejection cone, with the nozzle-to-sample distance set to 8.5 cm. A 5 s burst at 1 bar

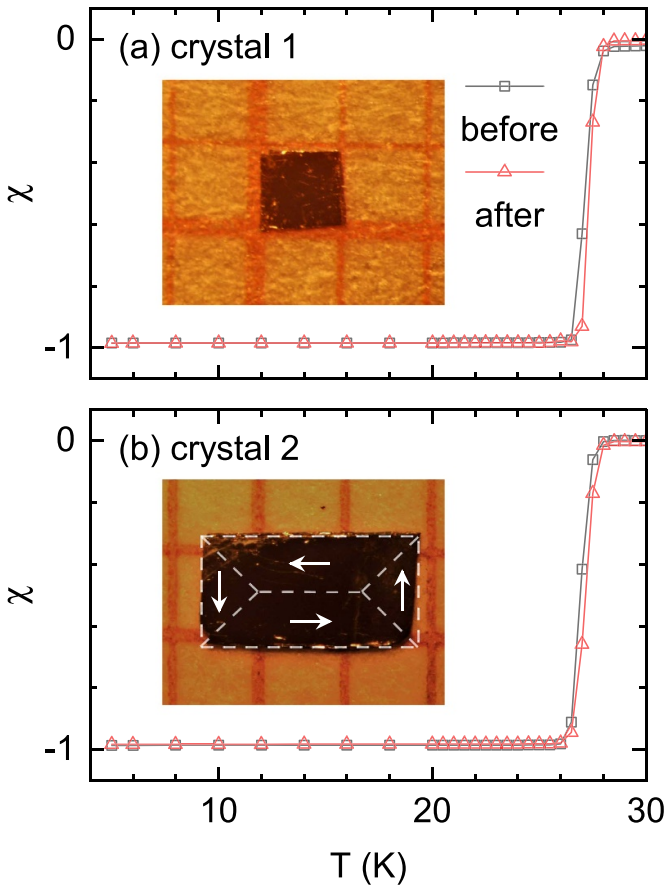

Figure 2. Magnetic susceptibility vs temperature for the $BaFe_2(As_{1-x}P_x)_2$ crystals studied, measured before and after the surface treatment. The crystals have T_c values about 27 K and transition widths under 1 K, evidencing excellent stoichiometric purity, which was not affected by the surface treatment. Photographs of the samples are included in the insets. The drawing on crystal 2 indicates the critical-state electrical current distribution used to evaluate (3).

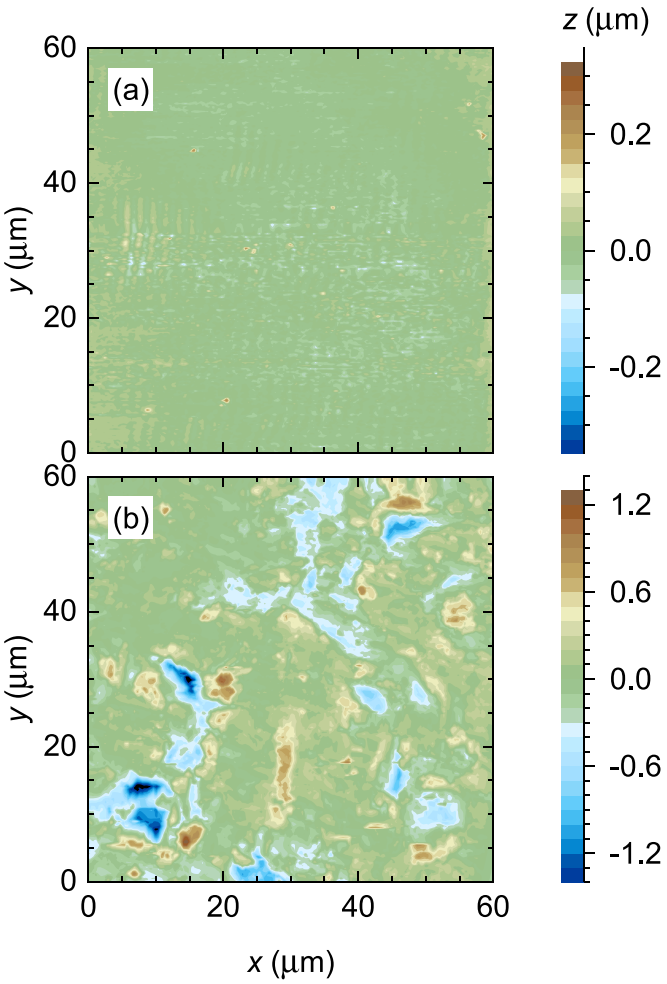

Figure 3. Example of AFM micrographs of the crystal surfaces (a) before and (b) after the abrasive blasting process. While in (a) the irregularities are limited to ± 0.1 μm, in (b) they extend up to ± 1.4 μm (note the difference in the scale).

Table 1. Characteristics of the crystals studied. The critical temperature T_c was obtained from low-field magnetic susceptibility measurements (figure 2). The c-axis lattice parameter c was obtained from x-ray diffraction analysis (figure 1). Both T_c and c agree with data in the literature for $BaFe_2(As_{1-x}P_x)_2$ with the same P content. The demagnetizing factor for $H \parallel c$, D_c, was estimated from the dimensions of the samples.

Crystal	T_c (K)	c (Å)	Size ($L_a \times L_b \times L_c$) ($mm^3$)	D_c	Mass (mg)	Sides etched
1	27.2	12.802(3)	$0.94 \times 0.94 \times 0.042$	0.933	0.230	1
2	26.9	12.795(3)	$2.48 \times 1.28 \times 0.070$	0.937	1.386	2

nozzle pressure was used to etch one of the *ab* surfaces of crystals 1 and 2. The reverse side of crystal 2 was also subjected to an identical etching process. After the sandblasting, the samples were carefully cleaned from sand residue. Atomic force microscopy (AFM) micrographs of the surface of the samples before and after the sandblasting process are shown in figure 3. As it can be seen, the sandblasting process creates defects typically ~ 5 μm wide and ~ 1 μm deep, covering most of the surface of the crystals. Figure 1 shows that the XRD peak positions and widths remain unchanged after sandblasting, indicating that the structural quality of the crystals is preserved. This was further confirmed by XRD measurements performed before and after sandblasting on another single crystal (crystal 3) with a higher 2 bar nozzle pressure (see figures S1 and S2 of the supplementary materials).

2.3. Magnetization measurements

The magnetization measurements were performed with a commercial SQUID magnetometer (MPMS-XL, Quantum Design) with the magnetic field applied perpendicular to the *ab* layers of the crystals. For this purpose, a quartz tube was used as a sample holder. The crystals were placed in a slit perpendicular to the tube axis, and glued with a small amount of GE varnish. Two plastic rods at the tube ends ensured an alignment of the c axis of the crystals with the applied magnetic field of about 0.1°.

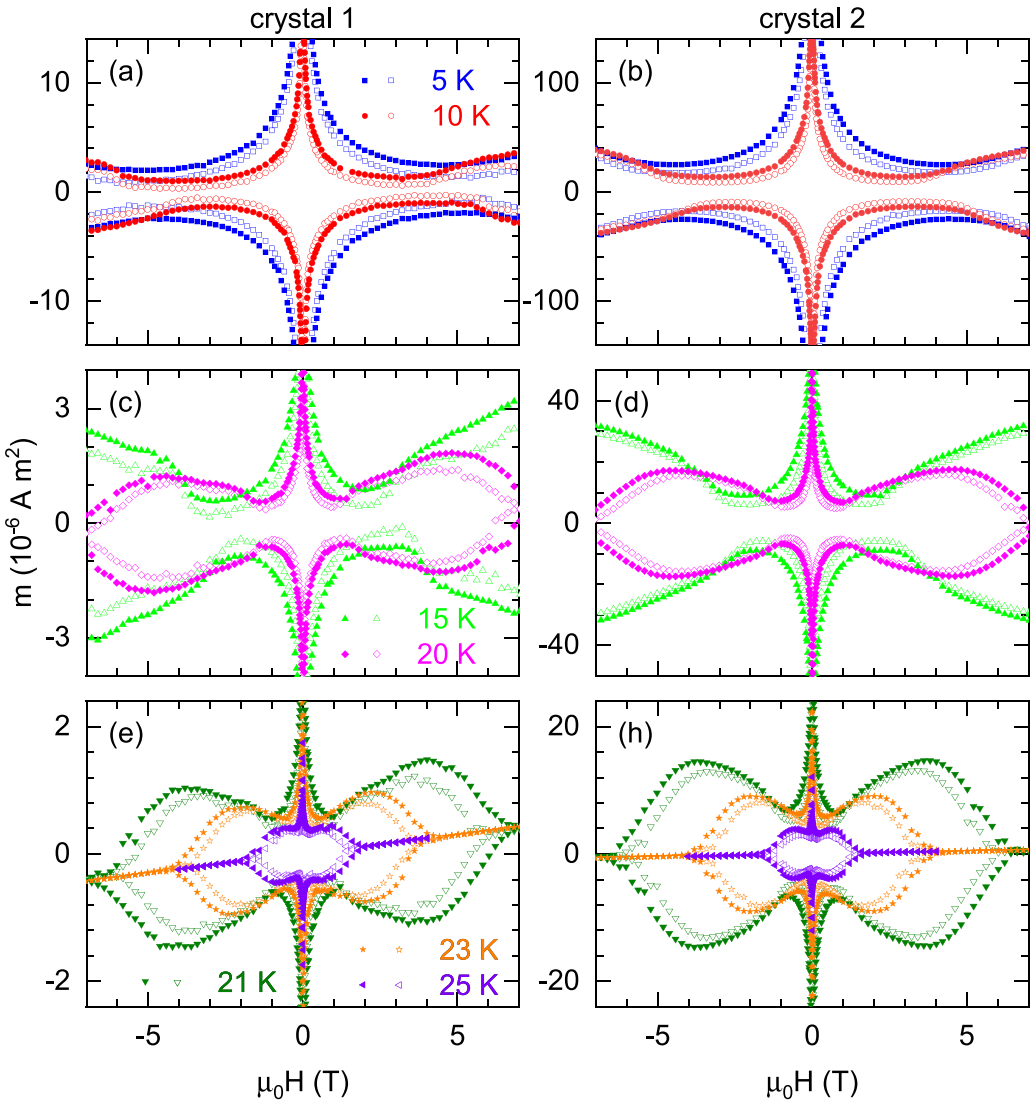

Figure 4. Isothermal $m(H)$ hysteresis curves for the two single crystals, before (open symbols) and after (solid symbols) sandblasting. Crystal 1 was sandblasted only from one side, while crystal 2 was sandblasted from both sides. As it can be seen, the hysteresis amplitude increased after the sandblasting process for both samples.

3. Results

The temperature dependence of the magnetic susceptibility χ, measured after zero-field-cooling (ZFC) with a low field ($\sim$0.3 mT) perpendicular to *ab* layers, is presented in figure 2. These data are corrected for demagnetizing effects by using the demagnetizing factors D calculated from the dimensions of the crystals (see table 1). As shown, χ is close to the ideal value of -1 at low temperatures, and the diamagnetic transition is very sharp (less than $\sim$1 K wide), which confirms the excellent stoichiometric quality of the crystals. The superconducting transition temperature, estimated from the diamagnetic transition midpoint, is $T_c \approx 27$ K (see table 1) typical of optimally-doped $BaFe_2(As_{1-x}P_x)_2$. [49] It is also worth noting that the surface treatment had little effect on the diamagnetic transition, indicating that it did not alter the homogeneity of the crystals.

To estimate the *ab*-layers' critical current density of the crystals before and after sandblasting, magnetic moment vs. magnetic field $m(H)$ hysteresis cycles were measured with $H \perp ab$ at different temperatures below T_c. These measurements were performed by first ZFC to the target temperature. The magnetic field was set using the so-called *hysteresis* charging mode (with the power supply continuously turned on), and data were acquired by using MPMS's *reciprocating sample option* (RSO), averaging 10 measuring cycles at 1 Hz. Figure 4 shows the $m(H)$ hysteresis loops obtained for both crystals before (open symbols) and after (solid symbols) sandblasting, evidencing a hysteresis amplitude increase at all the studied temperatures and for all magnetic fields. Near the irreversibility magnetic field H_{irr} (above which the hysteresis vanishes) the enhancement in the hysteresis amplitude (proportional to the surface I_c), is larger than the hysteresis amplitude before the surface treatment (proportional to the bulk I_c). It is worth noting that this compound presents a *second magnetization peak* (SMP), which can be clearly observed for temperatures above 15 K, consistently with previous measurements [15, 50, 51].

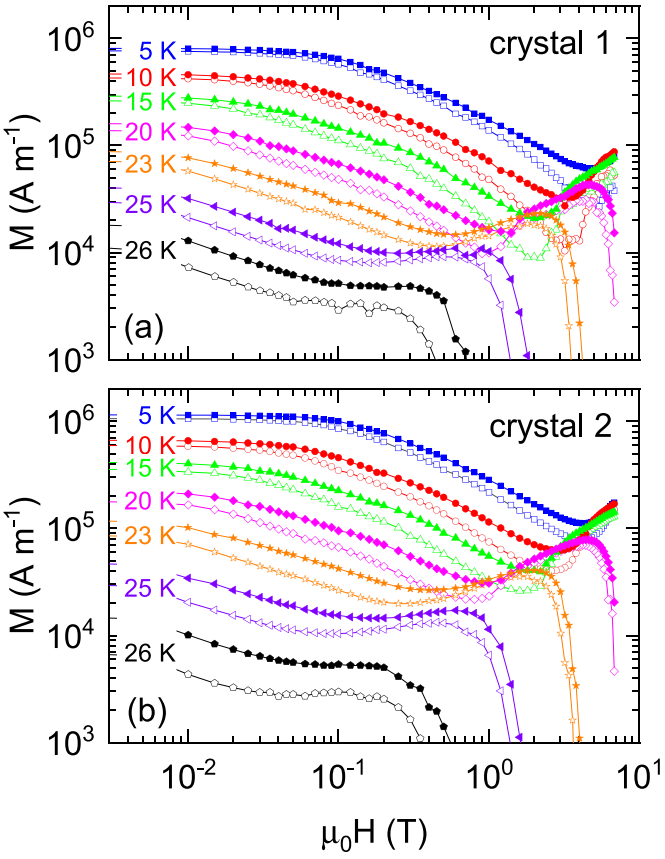

Figure 5. Detail of isothermal $M(H)$ cycles for $M, H > 0$, before (open symbols) and after sandblasting (solid symbols). The magnetization hysteresis increases at all applied magnetic fields, and is comparatively higher at temperatures closer to T_c. The irreversibility field H_{irr} was also increased, suggesting stronger pinning is taking place (see main text for details).

To better observe the effect of sandblasting at low fields and close to T_c, a detailed log-log representation of the upper-right branch of the hysteresis cycles for both samples is presented in figure 5. To facilitate comparison between both crystals with each other and with other samples in the literature, m is normalized by the volume of the crystals, and the normal-state paramagnetic signal was subtracted. As shown, the increase of the hysteresis amplitude due to the surface treatment extends to the low-H region and is more pronounced at temperatures closer to T_c. Finally, an increase of H_{irr} was also observed after the sandblasting process. In the following section, these effects will be interpreted in terms of an extra non-dissipative surface current made possible by the surface irregularities.

4. Discussion

4.1. Critical current enhancement

The *ab*-layers' critical current density J_c before the sandblasting process can be obtained from the $m(H)$ hysteresis loops measured with $H \perp ab$ using Bean's critical-state model [52, 53]. For a crystal with dimensions L_a, L_b and L_c (where $L_a > L_b > L_c$), this leads to [54]

$$J_c = \frac{2m_h/V}{L_b(1 - L_b/3L_a)}, \tag{1}$$

where $V = L_a L_b L_c$ and m_h is the amplitude of the $m(H)$ hysteresis loop. The temperature dependence of the resulting J_c at different applied magnetic fields is presented in figures 6(a) and (b) for both crystals. As shown, the J_c curves have a similar amplitude, temperature and magnetic field dependencies.

The increase in hysteresis amplitude after sandblasting (hereafter denoted as Δm_h) can be understood as the result of non-dissipative surface currents enabled by surface irregularities. The mechanism for the existence of such currents has been explained in previous works (see, e.g. [37] and references therein). These surface irregularities provide multiple ways for vortices to terminate at the sample surface while satisfying the boundary conditions, enabling a collective bending of the vortices that sustains an extra non-dissipative surface current. Defects with size of order λ are expected to induce this phenomenon, with λ being the characteristic length of the currents around vortices. The magnetic moment m_s due to these surface currents is given by

$$m_s = \frac{1}{2}\int_{\text{surface}} \left(\vec{r} \times \vec{K}\right) \mathrm{d}\vec{S}, \tag{2}$$

with $\vec{K}$ being the surface current density. In the critical state $\vec{K}$ corresponds to the critical surface current density $\vec{K}_c$, and the associated increase in hysteresis loop amplitude is given by

$$\Delta m_h = \left| \int_{\text{surface}} \left(\vec{r} \times \vec{K}_c\right) \mathrm{d}\vec{S} \right|. \tag{3}$$

To evaluate (3), the spatial dependence of $\vec{K}_c$ can be approximated by a Bean-like distribution, similar to the one expected for the underlying bulk current density (see diagram inset in figure 2(b)). For a crystal of dimensions L_a, L_b and L_c (where $L_a > L_b > L_c$) this leads to

$$\Delta m_h = \frac{K_c L_b^3}{2}\left(\frac{L_a}{L_b} - \frac{1}{3}\right) \tag{4}$$

per sandblasted surface.

The surface critical current density resulting from (4) and the Δm_h data in figure 4, is shown for both crystals in figures 6(c) and (d). For crystal 2 the effect of etching both sides was considered. As it can be seen, the result is very similar in both crystals, confirming the existence and reproducibility of the critical current enhancement by surface etching. The differences between the two samples can be attributed to some extent to the experimental uncertainty in obtaining K_c from the difference in the $m(H)$ hysteresis cycles before and after sandblasting, and to slight differences in the samples characteristics: the T_c value is ~0.3 K smaller for crystal 2, which may lead to a variation in the H_{c2} value [15].

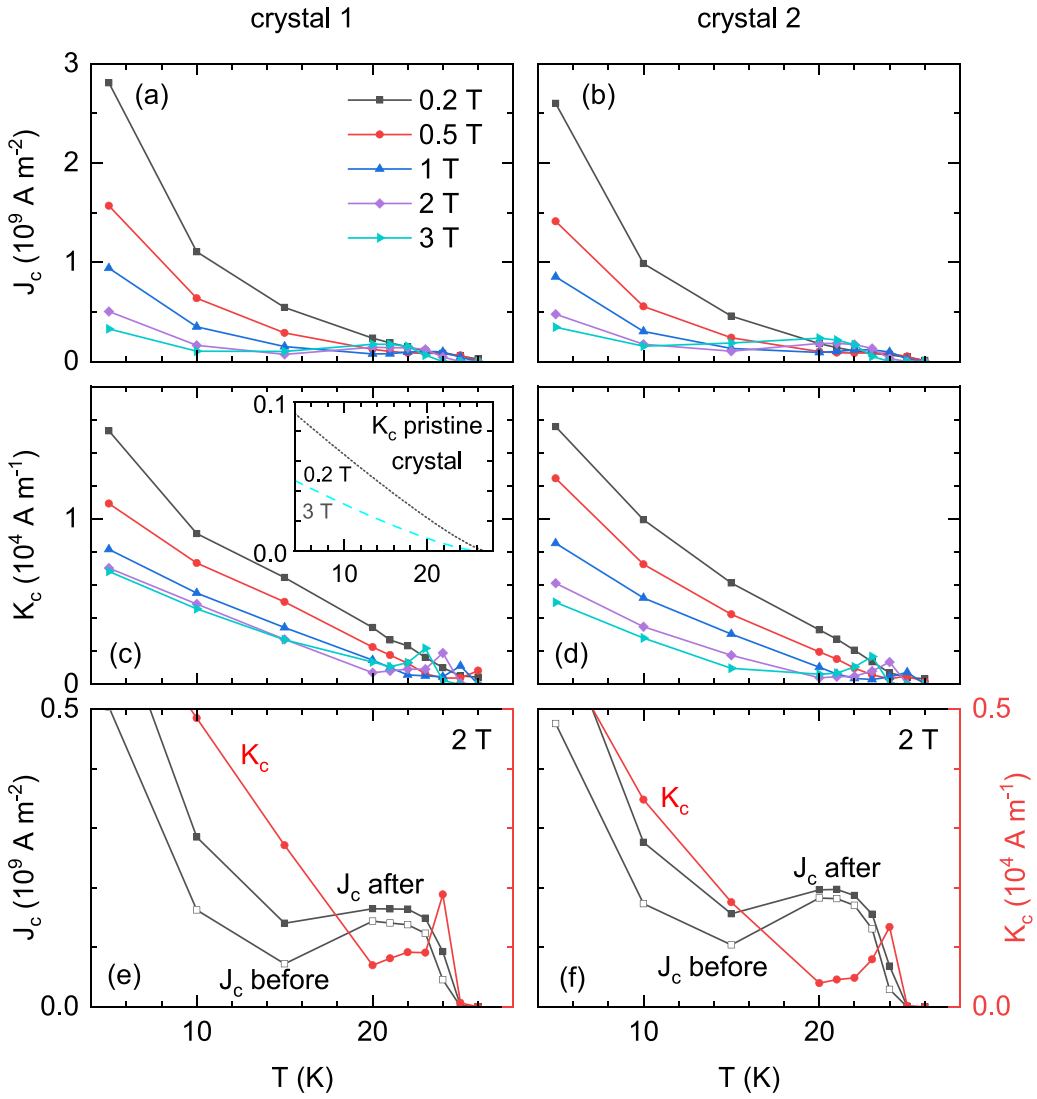

Figure 6. (a), (b) critical current density J_c before sandblasting, obtained by applying Bean's critical state model; (c), (d) surface critical current density K_c, obtained by assuming that all additional pinning occurs at the surface of the sample (4). The inset in (c) is an estimation of the surface critical current density of the pristine samples for 0.2 T and 3 T (see the main text for details). As it can be seen, the $K_c(T)$ curves follow a different trend than $J_c(T)$. This can be better observed in (e), (f), where the detail of $J_c(T)$ (black full squares) and $K_c(T)$ (red circles) close to T_c is shown, for an applied magnetic field of 2 T. The empty squares in (e), (f) correspond to $J_c(T)$ calculated after sandblasting, with the assumption that no surface currents are present. The equivalent comparison for 0.2, 0.5, 1 and 3 T are presented in figure S3 of the supplementary materials. As shown, the increase is not a constant factor, as it would be expected in first approximation for bulk pinning enhancement.

K_c decreases monotonically with T and H, but the T dependence is qualitatively different from the one of J_c: while K_c is roughly linear in all the studied temperature range, J_c grows faster at low temperatures. Moreover, J_c presents a broad maximum related to the second magnetization peak (SMP), which is absent in K_c at the same temperature (this can be better seen in the detail near T_c presented in figures 6(e) and (f). In turn, $K_c(T)$ presents a sharp peak just before vanishing, similar to the *peak effect* observed in the critical current of some low-T_c compounds [55, 56] and high-T_c cuprates [57], which has been attributed to the different T-dependence of pinning and elastic forces near $H_{c2}(T)$. [58] If $K_c(T)$ presented the broad peak characteristic of $J_c(T)$, perhaps it could be concluded that the surface roughness just contributes to enhance the conventional vortex pinning. The different $K_c(T)$ behavior suggests a different mechanism. This conclusion is further supported by the comparison in the next section of $K_c(T)$ with a theoretical result based on Mathieu-Simon theory for the maximum non-dissipative current that a rough surface can sustain.

4.2. Comparison with theoretical approaches

We will now discuss if the observed K_c behavior and amplitude is consistent with an estimate based on the Mathieu-Simon continuum theory of the mixed state for the non-dissipative current enabled by a rough surface. Let's assume that the external magnetic field B is applied along the z axis (parallel

to the crystal c axis), and the electrical current flows in the y direction. At a point in which the surface normal makes an angle α with the z axis, the vortices are bent in the xz plane so that the associated flux density ω makes an angle θ with z, given by $\tan\theta = \gamma^2 \tan\alpha$ (γ being the superconducting anisotropy factor). The flux density at the surface is $\omega = B/\cos\theta$. According to the Mathieu-Simon theory, the non dissipative local surface current density K is given by [37]

$$K = |M_x(\omega,\theta)|, \tag{5}$$

where $M_x(\omega,\theta)$ is the x component of the reversible magnetization of an anisotropic superconductor under a flux density ω at an angle θ relative to the crystal c axis. Using the result from [59] for the reversible magnetization vector of anisotropic superconductors in intermediate magnetic fields (far from both the upper and lower critical magnetic fields), we find that

$$K = \frac{\phi_0}{8\pi\mu_0\lambda_{ab}^2} \ln\left(\frac{\eta/b}{\sqrt{1+\gamma^2\tan^2\alpha}}\right) \frac{\tan\alpha}{\sqrt{1+\gamma^2\tan^2\alpha}}. \tag{6}$$

Here, λ_{ab} is the magnetic penetration depth for currents along the ab layers, $b \equiv B/B_{c2}^{\perp}$, where $B_{c2}^{\perp}$ is the upper critical field perpendicular to the ab layers, ϕ_0 is the magnetic flux quantum, μ_0 is the vacuum magnetic permeability, and η is a constant of order unity. For a given b, K has a maximum for some angle α_0. This can be seen in figure 7(a), where (6) is plotted against α for different b values, using parameters for optimally-doped $BaFe_2(As_{1-x}P_x)_2$ (see below). If the surface is sufficiently rugous, the vortices have many possible angles to terminate at the surface, and the critical surface current K_c will correspond to (6) evaluated with α_0. The condition $dK/d\alpha|_{\alpha_0} = 0$ leads to

$$\gamma^2\tan^2\alpha_0 = \frac{1}{2}W\left(\frac{2e^2\eta^2}{b^2}\right) - 1, \tag{7}$$

where $W(x)$ is Lambert's function (the inverse of xe^x), and e is Euler's constant. Substituting α_0 into (6) and simplifying, we finally obtain

$$K_c = \frac{\phi_0}{16\pi\mu_0\gamma\lambda_{ab}^2} W\left(\frac{2e^2\eta^2}{b^2}\right)\left[1 - \frac{2}{W\left(\frac{2e^2\eta^2}{b^2}\right)}\right]^{3/2}. \tag{8}$$

A similar calculation was obtained in [37] using Abrikosov's result for M_x close to the upper critical magnetic field, although this result is not applicable in the present case as the irreversibility field $H_{irr}(T) \sim 0.5H_{c2}(T)$ (see figure 8), impeding the study of K_c for fields close to H_{c2}.

Figure 7(b) shows the theoretical $K_c(T)$ for the same B values as in figure 6, evaluated by assuming a Ginzburg–Landau temperature dependence for the upper critical field $H_{c2}^{\perp}(T) = H_{c2}^{\perp\prime}(T - T_c)$ and the magnetic penetration depth $\lambda_{ab}(T) = \lambda_{ab}(0)/\sqrt{1 - T/T_c}$. The $\lambda_{ab}(0)$, $H_{c2}^{\perp\prime}$ and γ values used were obtained from from the data in [49] for the optimally-doped $BaFe_2(As_{1-x}P_x)_2$. Finally, the parameter η was approximated

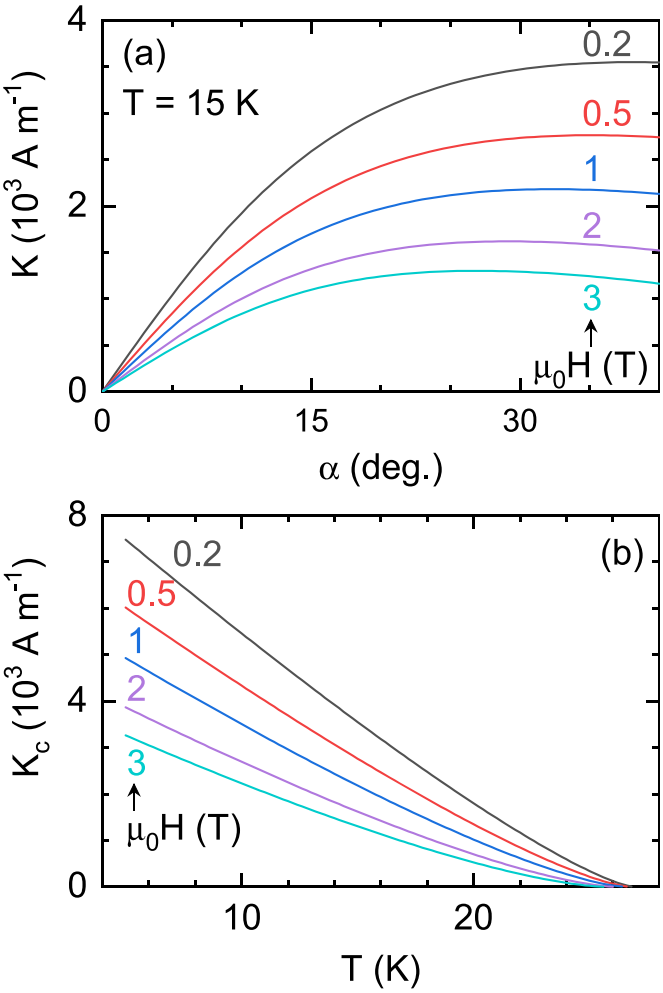

Figure 7. (a) Theoretical non-dissipative surface current density against α (the angle between the surface normal and the crystal c axis) for different applied magnetic fields. These curves were obtained from (6) with the superconducting parameters for optimally-doped $BaFe_2(As_{1-x}P_x)_2$ from [49]. As it can be seen, there is an angle α_0 for each field for which K is maximum. In a sufficiently rough surface, the critical current density corresponds to $K(\alpha_0)$ (8), which is plotted against T in (b). Note the good agreement with the experimental $K_c(T)$ shown in figures 6(c), (d).

to 1. As it can be seen, figure 7(b) resembles the experimental results for K_c summarized in figures 6(c) and (d), in both the temperature and magnetic field dependences (except for the peak effect observed just before vanishing). The difference in the amplitude (a factor of about two), could be probably attributed to the uncertainties in the superconducting parameters, in the geometry of the samples, and also to the initial roughness of the pristine crystals. The latter can be obtained from the AFM data of figure 3(a) from which we estimate that the maximum angles between the local surface normal and the crystal c-axis are up to $\alpha \sim 2$ degrees. The K_c obtained introducing this α value in equation (6) is shown in the inset of figure 6(c). As shown, the K_c of the pristine surfaces is about 10% of the experimental K_c value after sandblasting. Due to this effect, the K_c data in figures 6(c) and (d) estimated from the increase in the hysteresis of the $m(h)$ cycles, could actually be slightly

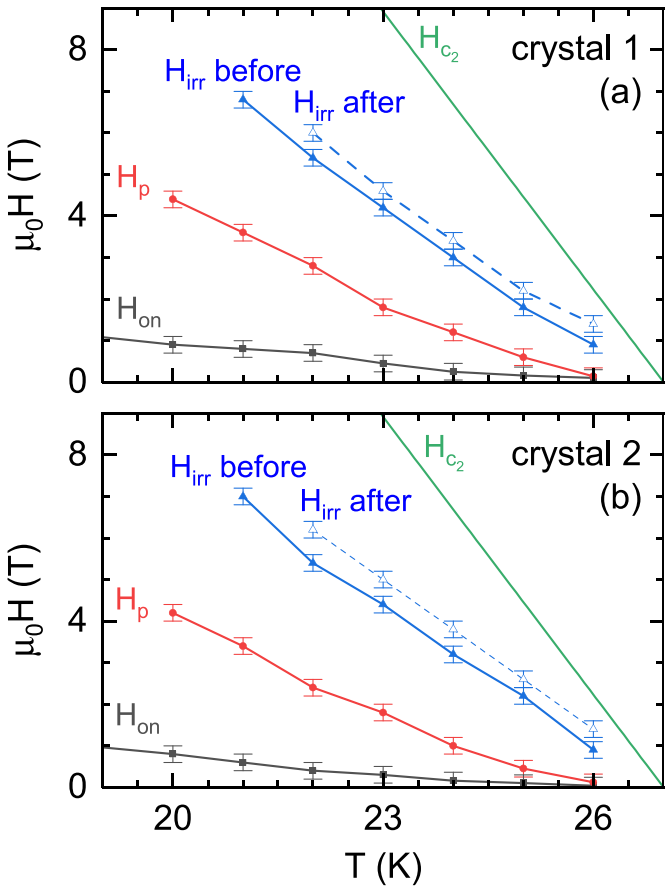

Figure 8. $H-T$ vortex phase diagrams for (a) crystal 1 and (b) crystal 2. H_{on} and H_p are, respectively, the onset and the maximum of the SMP before sandblasting. H_{irr} is the irreversibility field before (solid line) and after (dashed line) sandblasting. As a reference, we show the upper critical field line $H_{c2}(T)$, obtained from data in the literature [49].

larger, bringing the data closer to the theoretical estimation of figure 7(b).

4.3. H – T phase diagram and irreversibility field increase

In addition to the critical current enhancement, an increase of the irreversibility field H_{irr} was also observed after sandblasting, as shown in the $H-T$ phase diagrams presented in figure 8. The $H_{irr}(T)$ values in this figure were estimated from the $m(H)$ cycles as the magnetic field above which the magnetic moments $m(H^{\uparrow})$ and $m(H^{\downarrow})$ obtained by increasing and decreasing H respectively (i.e. the upper and lower branch of the hysteresis loops) coincide within the experimental resolution (see figure S4 of the supplementary materials for an example of this criterion). As it can be seen, the sandblasting process essentially shifts the $H_{irr}(T)$ line to ∼0.5 K higher temperatures. Equation (8) predicts that K_c should vanish at the $H_{c2}(T)$ line. However, this equation does not consider the effect of thermal fluctuations on the vortices, which play a non negligible role in these materials [45, 60–63]. For reference, the phase diagrams of figure 8 also include the onset and the maximum of the second magnetization peak (H_{on} and H_p, respectively), and the upper critical field line estimated from the data in [49]. For completeness, figure S5 of the supplementary materials shows an analysis of the pinning force in terms of Dew-Hughes model using the calculated H_{irr} values, in which no notable differences can be observed after the surface treatment.

5. Conclusions

The increase in vortex pinning induced by the addition of surface rugosity through abrasive sandblasting was studied in high-quality single crystals of optimally-doped $BaFe_2(As_{1-x}P_x)_2$. The effect on the critical current was investigated by measuring isothermal $m(H)$ hysteresis cycles with H perpendicular to the etched surfaces (i.e. the *ab* layers of the crystals), before and after the sandblasting process. A significant increase in the amplitude of the hysteresis loops was observed for both samples and at all temperatures. This increase is attributed to the presence of a non-dissipative surface current density K_c, which is associated with a collective bending of the vortex lattice close to the surface of the crystals. K_c presents a temperature dependence qualitatively different from that of J_c, estimated from the $m(H)$ cycles measured before sandblasting. However, $K_c(T)_H$ is in good agreement with a theoretical estimate for the maximum non-dissipative current that a rough surface can sustain, based on the Mathieu-Simon continuum theory of the vortex state. A slight increase of the irreversibility field $H_{irr}(T)$ was also observed after sandblasting. Finally, our measurements revealed a sharp increase in $K_c(T)$ just before vanishing (the so called *peak effect*), which is not present in $J_c(T)$, suggesting that surface roughness is among the causes that promote its appearance. In addition to its fundamental interest, the I_c enhancement by surface irregularities could also be useful to complement bulk pinning enhancement procedures in the development of FeSC thin films or tapes for electrical transport applications.

Data availability statement

The data that support the findings of this study are available upon reasonable request from the authors. All data that support the findings of this study are included within the article (and any supplementary files)

Acknowledgments

This work was supported by the Agencia Estatal de Investigación (AEI) through project PID2019-104296GB-I00. I F Llovo acknowledges financial support from Xunta de Galicia through Grant ED481A-2020/149. H Q Luo is supported by the National Key Research and Development Program of China (Grants Nos. 2018YFA0704200 and 2023YFA1406100), the Strategic Priority Research Program (B) of the CAS (Grants Nos. XDB25000000 and XDB33000000), and the Youth Innovation Promotion Association of CAS (Grant No. Y202001). The research at HangZhou Normal University is supported by the

Open Project of Guangdong Provincial Key Laboratory of Magnetoelectric Physics and Devices (Grant No. 2022B1212010008), Startup Project of HangZhou Normal University (Grant No. 2020QDL026) and Natural Science Foundation of Zhejiang Province (Grant No. LY22A040009). We acknowledge F Bonfiglio, who was an undergraduate student at the time, for his help in earlier studies related to this paper, which are not included in the present work. Authors would like to thank the use of RIAIDT-USC analytical facilities.

ORCID iDs

I F Llovo https://orcid.org/0000-0002-8413-0034
J Mosqueira https://orcid.org/0000-0002-8639-2329
Huiqian Luo https://orcid.org/0000-0003-1514-0041
Shiliang Li https://orcid.org/0000-0001-7922-3730

References

[1] Kamihara Y, Watanabe T, Hirano M and Hosono H 2008 Iron-based layered superconductor La[$O_{1-x}F_x$]FeAs ($x = 0.05 - 0.12$) with $T_c = 26$ K *J. Am. Chem. Soc.* **130** 3296–7
[2] Johnston D C 2010 The puzzle of high temperature superconductivity in layered iron pnictides and chalcogenides *Adv. Phys.* **59** 803–1061
[3] Stewart G R 2011 Superconductivity in iron compounds *Rev. Mod. Phys.* **83** 1589–652
[4] Ishida K, Nakai Y and Hosono H 2009 To what extent iron-pnictide new superconductors have been clarified: a progress report *J. Phys. Soc. Japan* **78** 062001
[5] Wang F and Lee D-H 2011 The electron-pairing mechanism of iron-based superconductors *Science* **332** 200–4
[6] Rey R I, Ramos-Álvarez A, Mosqueira J, Salem-Sugui S Jr, Alvarenga A D, Luo H-Q, Lu X-Y, Zhang R and Vidal F 2014 Direct measurement of the temperature dependence of the magnetic penetration depth in Ba($Fe_{1-x}Ni_x$)$_2As_2$ superconductors *Supercond. Sci. Technol.* **27** 055015
[7] Pallecchi I, Caglieris F and Putti M 2016 Thermoelectric properties of iron-based superconductors and parent compounds *Supercond. Sci. Technol.* **29** 073002
[8] Maksimov E G *et al* 2011 Two-band Bardeen-Cooper-Schrieffer superconducting state of the iron pnictide compound Ba($Fe_{0.9}Co_{0.1}$)$_2As_2$ *Phys. Rev.* B **83** 140502
[9] Hardy F, Wolf T, Fisher R A, Eder R, Schweiss P, Adelmann P, Löhneysen H V and Meingast C 2010 Calorimetric evidence of multiband superconductivity in Ba($Fe_{0.925}Co_{0.075}$)$_2As_2$ single crystals *Phys. Rev.* B **81** 060501
[10] Hunte F, Jaroszynski J, Gurevich A, Larbalestier D C, Jin R, Sefat A S, McGuire M A, Sales B C, Christen D K and Mandrus D 2008 Two-band superconductivity in $LaFeAsO_{0.89}F_{0.11}$ at very high magnetic fields *Nature* **453** 903–5
[11] Gurevich A 2011 Iron-based superconductors at high magnetic fields *Rep. Prog. Phys.* **74** 124501
[12] Xing X, Zhou W, Wang J, Zhu Z, Zhang Y, Zhou N, Qian B, Xu X and Shi Z 2017 Two-band and Pauli-limiting effects on the upper critical field of 112-type iron pnictide superconductors *Sci. Rep.* **7** 45943
[13] Llovo I F, Carballeira C, Sóñora D, Pereiro A, Ponte J J, Salem-Sugui S, Sefat A S and Mosqueira J 2021 Multiband effects on the upper critical field angular dependence of 122-family iron pnictide superconductors *Sci. Rep.* **11** 11526
[14] Miura M, Maiorov B, Kato T, Shimode T, Wada K, Adachi S and Tanabe K 2013 Strongly enhanced flux pinning in one-step deposition of $BaFe_2(As_{0.66}P_{0.33})_2$ superconductor films with uniformly dispersed $BaZrO_3$ nanoparticles *Nat. Commun.* **4** 2499
[15] Ishida S, Song D, Ogino H, Iyo A, Eisaki H, Nakajima M, Shimoyama J-I and Eisterer M 2017 Doping-dependent critical current properties in K, Co and P-doped $BaFe_2As_2$ single crystals *Phys. Rev.* B **95** 014517
[16] Mohan S, Taen T, Yagyuda H, Nakajima Y, Tamegai T, Katase T, Hiramatsu H and Hosono H 2010 Transport and magnetic properties of Co-doped $BaFe_2As_2$ epitaxial thin films grown on MgO substrate *Supercond. Sci. Technol.* **23** 105016
[17] Sakoda M, Iida K and Naito M 2018 Recent progress in thin-film growth of Fe-based superconductors: superior superconductivity achieved by thin films *Supercond. Sci. Technol.* **31** 093001
[18] Talantsev E F 2019 Evaluation of a practical level of critical current densities in pnictides and recently discovered superconductors *Supercond. Sci. Technol.* **32** 084007
[19] Katase T, Ishimaru Y, Tsukamoto A, Hiramatsu H, Kamiya T, Tanabe K and Hosono H 2011 Advantageous grain boundaries in iron pnictide superconductors *Nat. Commun.* **2** 409
[20] Hosono H, Yamamoto A, Hiramatsu H and Ma Y 2018 Recent advances in iron-based superconductors toward applications *Mater. Today* **21** 278–302
[21] Yao C and Ma Y 2019 Recent breakthrough development in iron-based superconducting wires for practical applications *Supercond. Sci. Technol.* **32** 023002
[22] Pyon S, Miyawaki D, Tamegai T, Awaji S, Kito H, Ishida S and Yoshida Y 2020 Enhancement of critical current density in (Ba,Na)Fe_2As_2 round wires using high-pressure sintering, *Supercond. Sci. Technol.* **33** 065001
[23] Yao C and Ma Y 2021 Superconducting materials: challenges and opportunities for large-scale applications *iScience* **24** 102541
[24] Zhang X and Ma Y 2022 Progress in the development of the 122-type IBS wires *Superconductivity* **2** 100010
[25] Weiss J D, Yamamoto A, Polyanskii A A, Richardson R B, Larbalestier D C and Hellstrom E E 2015 Demonstration of an iron-pnictide bulk superconducting magnet capable of trapping over 1 T *Supercond. Sci. Technol.* **28** 112001
[26] Eisterer M 2017 Radiation effects on iron-based superconductors *Supercond. Sci. Technol.* **31** 013001
[27] Maiorov B, Katase T, Usov I O, Weigand M, Civale L, Hiramatsu H and Hosono H 2012 Competition and cooperation of pinning by extrinsic point-like defects and intrinsic strong columnar defects in $BaFe_2As_2$ thin films *Phys. Rev.* B **86** 094513
[28] Taen T, Nakajima Y, Tamegai T and Kitamura H 2012 Enhancement of critical current density and vortex activation energy in proton-irradiated Co-doped $BaFe_2As_2$ *Phys. Rev.* B **86** 094527
[29] Torsello D, Gerbaldo R, Gozzelino L, Laviano F, Takahashi A, Park A, Pyon S, Ichinose A, Tamegai T and Ghigo G 2020 Twofold role of columnar defects in iron based superconductors *Supercond. Sci. Technol.* **33** 094012
[30] Nakajima Y, Tsuchiya Y, Taen T, Yagyuda H, Tamegai T, Okayasu S, Sasase M, Kitamura H and Murakami T 2010 Critical current densities and flux creep rate in Co-doped $BaFe_2As_2$ with columnar defects introduced by heavy-ion irradiation *Physica* C **470** 1103–5
[31] Otabe E S, Myose K, Murakami K, Kiuchi M, Matsushita T, Ge J, Ni B, Nakajima Y and Tamegai T 2012 Condensation

energy density properties of Ba-122 pnictide superconductor with columnar defects introduced by heavy-ion irradiation *Phys. Proc.* **36** 693–7
[32] Sato H, Hiramatsu H, Kamiya T and Hosono H 2016 Enhanced critical-current in P-doped $BaFe_2As_2$ thin films on metal substrates arising from poorly aligned grain boundaries *Sci. Rep.* **6** 36828
[33] Hiramatsu H, Sato H, Kamiya T and Hosono H 2017 $BaFe_2(As_1 - xP_x)_2$ $(x = 0.22 - 0.42)$ thin films grown on practical metal–tape substrates and their critical current densities *Supercond. Sci. Technol.* **30** 044003
[34] Tarantini C, Lee S, Kametani F, Jiang J, Weiss J D, Jaroszynski J, Folkman C M, Hellstrom E E, Eom C B and Larbalestier D C 2012 Artificial and self-assembled vortex-pinning centers in superconducting $Ba(Fe_{1-x}Co_x)_2As_2$ thin films as a route to obtaining very high critical-current densities *Phys. Rev.* B **86** 214504
[35] Lee S *et al* 2013 Artificially engineered superlattices of pnictide superconductors *Nat. Mater.* **12** 392–6
[36] Mathieu P and Simon Y 1988 Phenomenological theory of vortex motion in type-II superconductors *Europhys. Lett.* **5** 67
[37] Lazard G, Mathieu P, Plaçais B, Mosqueira J, Simon Y, Guilpin C and Vacquier G 2002 Critical currents in the anisotropic superconductor $2H - NbSe_2$: evidence for an upper bound of the surface critical-current density *Phys. Rev.* B **65** 064518
[38] Aburas M, Pautrat A and Bellido N 2016 Change of surface critical current in the surface superconductivity and mixed states of superconducting niobium *Supercond. Sci. Technol.* **30** 015009
[39] Casalbuoni S, Knabbe E, Kötzler J, Lilje L, von Sawilski L, Schmüser P and Steffen B 2005 Surface superconductivity in niobium for superconducting RF cavities *Nucl. Instrum. Methods Phys. Res.* **538** 45–64
[40] Sung Z-H, Dzyuba A, Lee P J, Larbalestier D C and Cooley L D 2015 Evidence of incomplete annealing at 800 °C and the effects of 120 °C baking on the crystal orientation and the surface superconducting properties of cold-worked and chemically polished Nb *Supercond. Sci. Technol.* **28** 075003
[41] Cubero A, Mart inez E, Angurel L, de la Fuente G, Navarro R, Legall H, Krüger J and Bonse J 2020 Effects of laser-induced periodic surface structures on the superconducting properties of niobium *Appl. Surf. Sci.* **508** 145140
[42] Cubero A, Mart inez E, Angurel L, de la Fuente G, Navarro R, Legall H, Krüger J and Bonse J 2020 Surface superconductivity changes of niobium sheets by femtosecond laser-induced periodic nanostructures *Nanomaterials* **10** 2525
[43] Nakajima M, Uchida S-i, Kihou K, Lee C-H, Iyo A and Eisaki H 2012 Growth of $BaFe_2(As_{1-x}P_x)_2$ single crystals $(0 \leqslant x \leqslant 1)$ by Ba_2As_3/Ba_2P_3-flux method *J. Phys. Soc. Japan* **81** 104710
[44] Hu D *et al* 2015 Structural and magnetic phase transitions near optimal superconductivity in $BaFe_2(As_{1-x}P_x)_2$ *Phys. Rev. Lett.* **114** 157002
[45] Ramos-Álvarez A, Mosqueira J, Vidal F, Hu D, Chen G, Luo H and Li S 2015 Superconducting fluctuations in isovalently substituted $BaFe_2(As_{1-x}P_x)_2$: possible observation of multiband effects *Phys. Rev.* B **92** 094508
[46] Jiang S, Xing H, Xuan G, Wang C, Ren Z, Feng C, Dai J, Xu Z and Cao G 2009 Superconductivity up to 30 K in the vicinity of the quantum critical point in $BaFe_2(As_{1-x}P_x)_2$ *J. Phys. Condens. Matter* **21** 382203
[47] Goh S K, Nakai Y, Ishida K, Klintberg L E, Ihara Y, Kasahara S, Shibauchi T, Matsuda Y and Terashima T 2010 Anisotropic superconducting properties of optimally doped $BaFe_2(As_0.65P_0.35)_2$ under pressure *Phys. Rev.* B **82** 094502
[48] Ishikado M, Kodama K, Kajimoto R, Nakamura M, Inamura Y, Wakimoto S, Iyo A, Eisaki H, Arai M and Shamoto S 2011 Inelastic neutron scattering on iron-based superconductor $BaFe_2(As,P)_2$ *Physica* C **471** 643–6
[49] Chaparro C, Fang L, Claus H, Rydh A, Crabtree G W, Stanev V, Kwok W K and Welp U 2012 Doping dependence of the specific heat of single-crystal $BaFe_2(As_{1-x}P_x)_2$ *Phys. Rev.* B **85** 184525
[50] Salem-Sugui S, Mosqueira J, Alvarenga A D, Sóñora D, Herculano E P, Hu D, Chen G and Luo H 2015 Observation of an anomalous peak in isofield M(T) curves in $BaFe_2(As_{0.68}P_{0.32})_2$ suggesting a phase transition in the irreversible regime *Supercond. Sci. Technol.* **28** 055017
[51] Salem-Sugui S, Mosqueira J, Alvarenga A D, Sóñora D, Crisan A, Ionescu A M, Sundar S, Hu D, Li S-L and Luo H-Q 2017 Vortex–glass state in the isovalent optimally doped pnictide superconductor $BaFe_2(As_0.68P_0.32)_2$ *Supercond. Sci. Technol.* **30** 055003
[52] Bean C P 1962 Magnetization of hard superconductors *Phys. Rev. Lett.* **8** 250–3
[53] Bean C P 1964 Magnetization of high-field superconductors *Rev. Mod. Phys.* **36** 31–39
[54] Poole C P, Farach H A, Creswick R J and Prozorov R 2007 *Superconductivity* 2nd edn (Academic)
[55] Bhattacharya S and Higgins M J 1994 Peak effect and anomalous flow behavior of a flux-line lattice *Phys. Rev.* B **49** 10005–8
[56] Xiao Z L, Andrei E Y, Shuk P and Greenblatt M 2000 Equilibration and dynamic phase transitions of a driven vortex lattice *Phys. Rev. Lett.* **85** 3265–8
[57] Kwok W K, Fendrich J A, Van der Beek C J and Crabtree G W 1994 Peak effect as a precursor to vortex lattice melting in single crystal $YBa_2Cu_3O_{7-\delta}$ *Phys. Rev. Lett.* **73** 2614–7
[58] Xu X B, Fangohr H, Xu X N, Gu M, Wang Z H, Ji S M, Ding S Y, Shi D Q and Dou S X 2008 Peak effect in the critical current of type II superconductors with strong magnetic vortex pinning *Phys. Rev. Lett.* **101** 147002
[59] Kogan V G, Fang M M and Mitra S 1988 Reversible magnetization of high-T_c materials in intermediate fields *Phys. Rev.* B **38** 11958–61
[60] Salem-Sugui S, Ghivelder L, Alvarenga A D, Pimentel J L, Luo H, Wang Z and Wen H-H 2009 Superconducting fluctuations in the reversible magnetization of the iron-pnictide $Ba_{1-x}K_xFe_2As_2$ *Phys. Rev.* B **80** 014518
[61] Mosqueira J, Dancausa J D, Vidal F, Salem-Sugui S, Alvarenga A D, Luo H-Q, Wang Z-S and Wen H-H 2011 Observation of anisotropic diamagnetism above the superconducting transition in iron pnictide $Ba_{1-x}K_xFe_2As_2$ single crystals due to thermodynamic fluctuations *Phys. Rev.* B **83** 094519
[62] Rey R I, Carballeira C, Mosqueira J, Salem-Sugui Jr S, Alvarenga A D, Luo H-Q, Lu X-Y, Chen Y-C and Vidal F 2013 Measurements of the fluctuation-induced in-plane magnetoconductivity at high reduced temperatures and magnetic fields in the iron arsenide $BaFe_{2-x}Ni_xAs_2$ *Supercond. Sci. Technol.* **26** 055004
[63] Rey R I, Ramos- Alvarez A, Carballeira C, Mosqueira J, Vidal F, Salem-Sugui S, Alvarenga A D, Zhang R and Luo H 2014 Measurements of the superconducting fluctuations in optimally doped $BaFe_{2-x}Ni_xAs_2$ under high magnetic fields: probing the 3D-anisotropic Ginzburg–Landau approach *Supercond. Sci. Technol.* **27** 075001